ALaDyn: A High-Accuracy PIC Code for the Maxwell–Vlasov Equations

Carlo Benedetti, Andrea Sgattoni, Giorgio Turchetti, and Pasquale Londrillo

***Abstract*—In this paper, we present Acceleration by Laser and Dynamics of charged particles (ALaDyn), a particle-in-cell code, to investigate the interaction of a laser pulse with a preformed plasma and/or an externally injected beam. The code, fully parallelized, works in 1-D, 2-D, and 3-D Cartesian geometry, and it is based on compact high-order finite-difference schemes ensuring higher spectral accuracy. We discuss the features, the performances, and the validation tests of the code. We finally present a preliminary application on a physically relevant case based on the PLASMON-X experiment of the CNR-INFN.**

***Index Terms*—Implicit compact schemes, laser–plasma interaction, particle-in-cell (PIC) simulations.**

I. Introduction

PLASMA-BASED acceleration [1] has received much theoretical and experimental attention due to the high longitudinal electric fields that can be excited in a plasma without the limitations found in conventional accelerators. Electron beams up to 1 GeV with a low energy spread and small emittance have been obtained using the laser-wakefield acceleration scheme (LWFA), and the energy doubling of 42-GeV electrons from the SLAC linac in a meter-scale plasma has been recently achieved (PWFA) [2]–[6]. Rapid progresses are expected from the new laser generation with multiterawatt pulses of a few femtoseconds length.

The activity of the PLASMON-X experiment [7], a joint project of the CNR-INFN, is closely related to these topics. The main purposes of the project are as follows: 1) acceleration of electrons auto or externally injected into plasma electron waves excited by ultrashort ($\sim$20 fs) high-power (100–300 TW) laser pulses (laser FLAME) and 2) development of a monochromatic and tunable X-ray source (20–1000 keV) based upon Thomson scattering of laser pulses by relativistic electrons.

The basic physical phenomena of the interaction of a laser pulse and/or a charged beam with a plasma are understood [8], but a complete 3-D relativistic treatment which deals with experiments, allowing also to have some insight in the details of the underlying physics, requires a numerical approach. Several codes (particle in cell, PIC) have been already proposed in this respect [9]–[11]; in all the cases, the description of the fields/particles dynamics is second-order accurate (fields on a Yee lattice evolved with the leap-frog scheme and particles push with the Boris algorithm) [12].

The relativistic PIC-code ALaDyn [13] we are presenting has been developed at the Department of Physics of the Bologna University in the framework of the PLASMON-X collaboration. The code, fully parallelized with MPI, is a suite of functions written in C (an independent FORTRAN90 version is also available) and organized into a library. The key points in developing a numerical scheme to solve the Maxwell–Vlasov equations concern the fields' propagation and the particles' evolution. A small error in the dispersion relation and phase velocity of the electromagnetic wave jointly with a reliable approximation to the characteristics of the phase-space-distribution function can only be obtained in the fully 3-D case by a PIC code. In ALaDyn, we have implemented high-order discretization methods for the differential operators in configuration space (compact finite-differences schemes [14]) jointly with accurate time-integration schemes (high-order Runge–Kutta). Using high-order schemes, we can adopt, for a fixed accuracy, a coarser computational grid (allowing the use of a higher particles-per-cell number) and a larger time step as compared to standard PIC codes. The code can run in one, two, and three spatial dimensions in Cartesian geometry. The parallelization is achieved through a simple longitudinal-domain decomposition (dynamically updated); the planning of a more sophisticated decomposition strategy is underway. In laser–plasma interactions, the great disparity in the temporal/spatial scales involved in the simulation leads to large computational requirements both in terms of CPU time and memory need. In general, we need to study the propagation of a short laser pulse (or a probe beam) through a plasma, which is several times longer than the pulse. Because only the region of the plasma near the laser pulse is of interest, in our code, the solution of the Maxwell equations is performed in a moving window which moves with the pulse. This allows us to save a considerable amount of memory. Another relevant feature of the code is the possibility to perform the simulations in a boosted Lorentz frame. Since the ranges of space and time scales spanned by a system are not invariant under Lorentz transformation, it can be proved that the existence of a reference frame (the boosted frame) where the imbalance between these scales is significantly reduced as compared to the laboratory frame, implying, in some case, the reduction of the simulation run time [15], [16]. The code has been designed and developed in order to be as flexible as possible. The background plasma can be completely defined by the user by simply adding the desired functions and structures. Several modules describing

Manuscript received November 19, 2007; revised March 5, 2008.

C. Benedetti, A. Sgattoni, and G. Turchetti are with the Dipartimento di Fisica, University di Bologna–INFN, 40126 Bologna, Italy (e-mail: benedetti@bo.infn.it).

P. Londrillo is with INAF, Osservatorio Astronomico di Bologna, 40127 Bologna, Italy.

Color versions of one or more of the figures in this paper are available online at http://ieeexplore.ieee.org.

Digital Object Identifier 10.1109/TPS.2008.927143

different types of laser pulses are already available (planar wave, focalized pulses in 2-D/3-D), but the user can easily add its own modules. The possibility to include external fields will be soon considered. An arbitrary number of particles species can be introduced in the simulation (e.g., electrons/ions of the plasma, electrons of the beam, test particles, etc.). The number of numerical particles associated to each specie can be set separately so that each species is represented by a suitable number of macroparticles. Concerning the interpolation of the fields at particles' position and the current deposition, linear and quadratic shape functions are available.

A crucial point is the validation of the code which can be achieved at different levels by comparison with the available analytical results and/or through the benchmarking with other Vlasov codes (PIC or fluid). The first step is testing the propagation of an electromagnetic pulse in the free space. The second one is to test the Maxwell–Liouville version of the code, where the particles move in the field of an assigned wave packet without affecting it. Finally, we can consider the fully self-consistent Maxwell–Vlasov version of the code in the case of classical electrostatic (plasma oscillations, Landau damping [17], two-streams instability) and electromagnetic (1-D solitons [21]) plasma-physics problems.

The rest of this paper is organized as follows. In Sections II and III, we describe in some details the algorithms and the features of ALaDyn. In Section IV, we discuss the validation tests. In Section V, we present the application of the code to a physically relevant case based on the PLASMON-X experiment. Finally, in Section VI, we summarize this paper and discuss future plans.

II. Basic Algorithms

We study the dynamics of the laser–plasma interaction in the mean field approximation. In this case, we have to solve the Vlasov equations for all the species jointly with the Maxwell equations for the fields

$$\frac{\partial f_s}{\partial t} + \mathbf{v}\cdot\frac{\partial f_s}{\partial \mathbf{r}} + q_s\left(\mathbf{E}+\frac{v}{c}\times\mathbf{B}\right)\cdot\frac{\partial f_s}{\partial \mathbf{p}} = 0 \qquad (1)$$

where f_s and q_s are, respectively, the phase-space distribution and the elementary charge for species s ($s =$ electrons, ions, etc.). The electric and magnetic fields $(\mathbf{E},\mathbf{B})$ satisfy

$$\frac{\partial \mathbf{B}}{\partial t} = -c\nabla\times\mathbf{E} \quad \frac{\partial \mathbf{E}}{\partial t} = c\nabla\times\mathbf{B} - 4\pi\mathbf{J} \qquad (2)$$

where the current density $\mathbf{J}$, defined as

$$\mathbf{J} = \sum_s q_s \int \mathbf{v} f_s(\mathbf{p},\mathbf{r},t)d\mathbf{p} \qquad (3)$$

couples the Vlasov [(1)] and the Maxwell equations [(2)]. The remaining two Maxwell

$$\nabla\cdot\mathbf{E} = 4\pi\rho \quad \nabla\cdot\mathbf{B} = 0 \qquad (4)$$

can be considered "initial conditions" for the system and remain satisfied for any time if they are satisfied at $t = 0$, provided that the local charge conservation holds, namely,

$$\frac{\partial \rho}{\partial t} + \nabla\cdot\mathbf{J} = 0. \qquad (5)$$

Considering the typical spatial/temporal scales involved in the laser–plasma interaction, the direct solution of (1), where f_s and the fields are discretized on a grid, is easily feasible only in the case of one spatial dimension (2-D phase space). The case with two spatial dimensions (4-D phase space) is already extremely demanding in terms of memory and CPU time, and it is clear that the fully 3-D case is beyond the present computer capabilities. Taking into account these difficulties, in ALaDyn, we solve (1) by using the PIC scheme. In the PIC technique, the (continuous) single-particle phase-space distribution f_s is sampled by a (possibly) large-number N_s of numerical particles according to

$$q_s f_s \to C_{N_s}\sum_{i=1}^{N_s} q_i \delta\left(\mathbf{r}-\mathbf{r}_i(t)\right)\delta\left(\mathbf{p}-\mathbf{p}_i(t)\right) \qquad (6)$$

where $\delta(\cdot)$ is the Dirac delta, q_i, $\mathbf{r}_i$, and $\mathbf{v}_i$ are, respectively, the charge and the coordinates of the ith numerical particle, and C_{N_s} is a normalization constant [22]. With this approximation, the characteristics of (1) are obtained by solving the following relativistic equations of motion:

$$\begin{cases} \frac{d\mathbf{r}_i}{dt} = \mathbf{v}_i \equiv \frac{\mathbf{p}_i}{m_i\gamma_i}, \\ \frac{d\mathbf{p}_i}{dt} = q_i\left(\mathbf{E}(\mathbf{r}_i,t) + \frac{\mathbf{v}_i}{c}\times\mathbf{B}(\mathbf{r}_i,t)\right), \qquad i = 1,\ldots,N_s \end{cases} \qquad (7)$$

γ_i and m_i being respectively the relativistic factor and the mass for the ith numerical particle (we set $q_i/m_i = q_s/m_s$). The main approximation in this approach is given by the evaluation of the self-consistent fields at the particle position (the same procedure applies to the current density), since the fields $\mathbf{E}$, $\mathbf{B}$ (and $\mathbf{J}$) are discretized on a spatial grid. The interpolation procedure, from particles position to grid points and vice versa, is equivalent to replace the delta function in (6) with a smooth function $S(\cdot)$ (shape function), $\delta(\mathbf{r}-\mathbf{r}_i) \to S(\mathbf{r}-\mathbf{r}_i)$. The choice of a suitable expression for S is important to keep under control the statistical noise which is always present in a PIC simulation due to the finite number of numerical particles exploited to sample the phase-space distribution.

The evolution of the electromagnetic fields is obtained by direct integration of (2). The curl operators in the right-hand side of (2) are represented by high-order compact finite-difference schemes [14]. These are implicit schemes which require the inversion of a band matrix on the grid. Letting f_i correspond to the value of the function $f(x)$ on the ith grid point $x_i = ih$, where h is the discretization step. The values f'_i which approximate the derivative $(df/dx)(x_i)$ in x_i are obtained from the following set of linear equations:

$$\begin{aligned} \alpha f'_{i-1} + f'_i + \alpha f'_{i+1} = {} & a\frac{f_{i+1}-f_{i-1}}{2h} \\ & + b\frac{f_{i+2}-f_{i-2}}{4h} \\ & + c\frac{f_{i+3}-f_{i-3}}{6h} \end{aligned} \qquad (8)$$

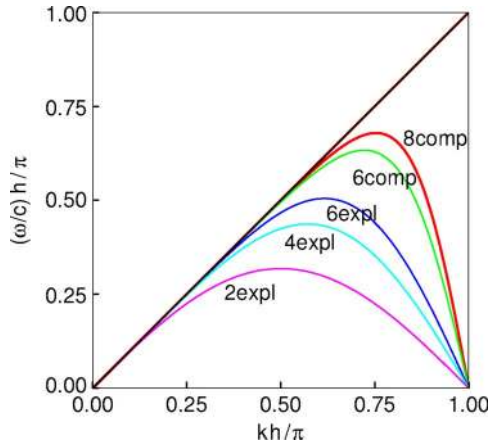

Fig. 1. Numerical-dispersion relation $\omega(k)$ for planar waves obtained with several finite-differences schemes as compared with (black plot) the exact solution $\omega(k) = ck$; h is the spatial discretization step.

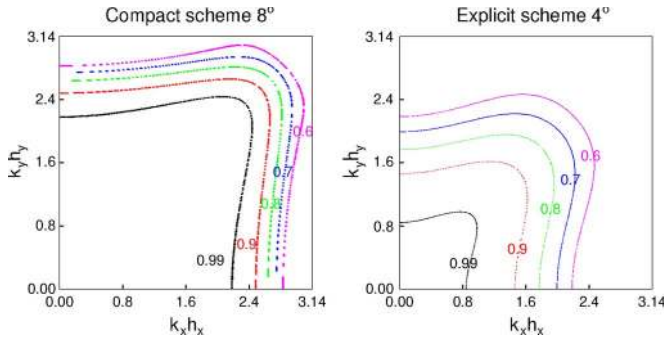

Fig. 2. Numerical values for the normalized phase velocity $v_p h/c$ of a plane wave in the (k_x, k_y) plane obtained (left panel) with a compact scheme and (right panel) with an explicit scheme.

where the relations between a, b, c, and α are derived by matching the Taylor-series coefficients of various orders. The "classical" second-order accurate expression for the derivatives is obtained setting $\alpha = b = c = 0$, $a = 1$. Casting (8) in vector form, we have

$$\mathbf{f}' = \mathcal{T}^{-1}\mathcal{U}\mathbf{f} \tag{9}$$

where $\mathcal{T}$ is a tridiagonal matrix and $\mathcal{U}$ is a band matrix. The increase in the computational cost to determine $\mathbf{f}'$ as compared to the second-order accurate expression is largely compensated by the improvement in the accuracy. In Fig. 1, we show the numerical dispersion relation $\omega(k)$ for planar waves obtained for implicit and explicit schemes at various order. We see that, even with few (approximately eight) points per wavelength, the compact high-order schemes provide a very good resolution of the phase velocity of the wave. With these schemes, we have also a global improvement of the isotropy in the wave phase velocity. In Fig. 2, we show the value of the normalized phase velocity v_{ph}/c for plane waves in the (k_x, k_y) plane for compact (left panel) and explicit (right panel) schemes. An increase in the accuracy of the spatial derivatives evaluation, which provides a better description of small-scale structures, requires high-order integration schemes in order to avoid instabilities. In `ALaDyn`, time integration, for both fields and particles, is carried out by using Runge–Kutta schemes on the fourth order

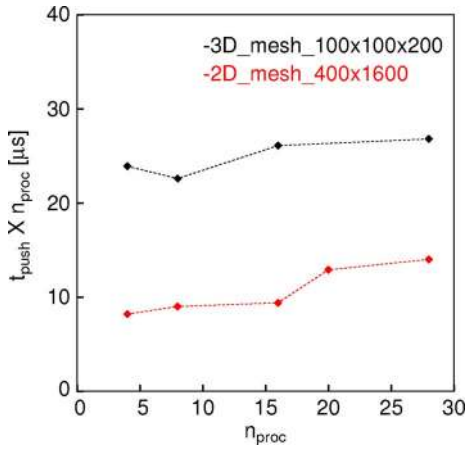

Fig. 3. Parallel scaling of `ALaDyn` (red) in the 2-D and (black) in the 3-D case. In 2-D, the computational mesh consisted of 400×1600 point (10 particles/cell). In the 3-D case, we have taken a mesh of $100 \times 100 \times 200$ points (10 particles/cell).

(but also schemes of second and third orders are available) [23]. The use of high-order algorithms in space and time allows us to adopt a coarser computational grid (allowing the use of a higher particles-per-cell number) and a larger time step as compared to standard second-order accurate PIC codes.

Another relevant point is the interpolation scheme adopted to evaluate the fields at particles' position and to perform the current deposition. High-order (greater or equal to third order) shape functions significantly reduce the statistical noise [24], but the computational costs in 2-D/3-D simulations seems to be quite high. In `ALaDyn`, the standard interpolation is done with second-order shape functions. In addition, linear-interpolation algorithms are available for quick and low-accuracy simulations.

III. Features of `ALaDyn`

The code `ALaDyn` is a library written in C. The basic functions have been independently rewritten by one of us in FORTRAN90 in order to highlight possible bugs in the code and test different solutions. `ALaDyn` works in one, two, and three spatial dimensions in Cartesian geometry. The dimensionality can be set at run time. The code has been parallelized with MPI. The parallelization strategy is based on the longitudinal-domain decomposition. The domains are dynamically updated in order to maintain an optimal load balance between the CPUs. We are also considering the implementation of a more general domain decomposition in order to improve the scalability of the code. In Fig. 3, we show the simulation time (in microseconds) corresponding to one particle push (with a fourth-order Runge–Kutta) multiplied by the number of processors (n_{proc}) for a given computational mesh as a function of n_{proc} in 2-D and in 3-D.

The great disparity in the spatial scales involved in the laser–plasma interaction makes the direct numerical simulation of this process very demanding in terms of memory and CPU-time requirements. The typical case is represented by the LWFA where a laser pulse of $\sim$10-μm length propagates through a plasma of several millimeters. Since only the region near the

laser pulse is of interest, the solution of the Maxwell equations is performed in a computational moving window, which follows the pulse. With the moving-window technique, only the fields around the laser pulse need to be stored and managed, allowing a considerable reduction in the memory need.

Another feature included in ALaDyn is the possibility to reduce the run-time of the simulation performing the calculations in a suitable reference frame. Since the space and time scales involved in the laser–plasma interaction are not invariant under Lorentz transformation, we can find a reference frame (the boosted Lorentz frame) in which the imbalance of these scales (and so the simulation run-time) is considerably reduced[1] as compared to the laboratory frame (for a detailed description of this technique, see [16] and the references therein). The principal drawbacks of this technique are related to the diagnostic (density plots, fields distribution), which is more difficult to perform due to the loss in the contemporaneity between the two reference frames.

Concerning the particles implementation in ALaDyn, several different types can be loaded in the simulation as in the following example.

```
/* Declaration of the species */
PARTICLES e_plsm, i_plsm, e_inj, e_test;
/* Creation of the species */
/* e_plsm: electrons of the plasma (active) */
createParticles(&e_plsm, ELECTRON, ...
/* i_plsm: ions of the plasma (virtual) */
createParticles(&i_plsm, ION, ...
/* e_inj: injected electron beam (active) */
createParticles(&e_inj, ELECTRON, ...
/* e_test: electrons as test particles
(passive, direct knowledge of each particle) */
createParticles(&e_test,
  ELECTRON AS TEST_PARTICLE, ...
```

The number of numerical particles associated to each species can be decided separately for each species by using the following function:

```
void setMacroparticlesNumber(
  PARTICLES *particles,
  int Nparticles, ...)
```

so that every particle family is described by the suitable number of numerical particles. The code has been developed in order to be as flexible as possible. The user can completely define the background plasma structure and profile by simply adding few C instructions as in the following example:

```
/* Plasma definition */
typedef struct {
  double L_rise, L_plateau, L_descent;
  double electron_density;
  double ion_density;
} PLASMA;
double plasmaProfile(double *position,
PARTICLES *particles, ...)
{
  /*
  This function returns the local value of
  the density for the species⟨particles⟩ in
  the position ⟨position⟩.
  */
  ....
}
```

Several modules describing different types of laser pulse have already been included in ALaDyn: planar wave with "$\cos^2$-like" longitudinal profile and linearly polarized and focalized pulses in 2-D and 3-D with Gaussian transversal profile. The user can easily add its own laser-pulse modules by linking the corresponding function.

Finally, we recall that two execution modes are available: FROM_MAXWELL_EQUATIONS and ANALYTICAL. In the former, the electromagnetic fields and the particles are self-consistently evolved; in the latter, the particles move in a prescribed field without affecting it.

IV. Validation Tests

The validation of an electromagnetic PIC code is not an easy task due to the highly nonlinear physics involved in the laser–matter interaction. Few are the known analytical solutions that can be taken as a reference, and the benchmarking with other codes (PIC or Vlasov fluid) is the only remaining option.

We present some validation tests performed with ALaDyn. If not stated elsewhere, in all the simulations presented, the spatial derivatives have been computed with an eighth-order compact scheme and the time integration using a fourth-order Runge–Kutta.

A. Propagation of a Focalized Pulse

We consider a focalized 3-D laser pulse linearly polarized ($\cos^2$-like longitudinal profile, Gaussian transversal profile) propagating in the free space along z-direction. The evolution of the pulse can be computed "analytically" by using FFT. In Fig. 4 (see the figure caption for the pulse parameters), we show the behavior of the transverse electric field ($E_x(x=0,y=0,z,t)$ obtained with ALaDyn using a grid with nine points/wavelength in the longitudinal direction and three points/wavelength in the transversal ones. Even with few points per wavelength, the agreement with the analytical solution is very good also for long times.

B. First Integral Conservation

In this case, we consider a test particle (electron) in a planar wave with finite length ($\cos^2$-like longitudinal profile, $\lambda_0 = 1\ \mu$m, $a_0 = eA_0/m_ec^2 = 1$). The energy conservation implies that $I = \gamma - u_z = \text{cost}$, where $u_z = p_z/m_ec$ and γ is the relativistic factor. For particles initially at rest, $I = 0$ and so $u_z = u_x^2/2$. In Fig. 5 (left panel), we show the behavior

[1]This applies mainly in the case of the propagation of a laser pulse in an underdense plasma.

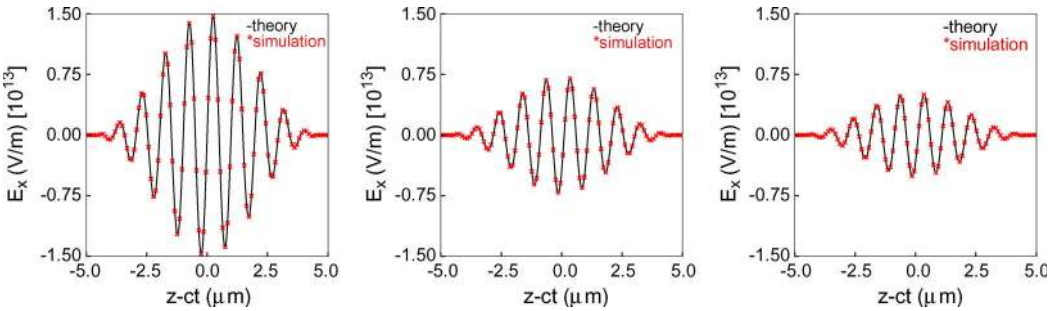

Fig. 4. Behaviour of $E_x(x=0,y=0,z,t)$ for $t=0$ (left), 208 (center), and 416 fs (right). The black plot is the analytical solution; the red diamonds are the solution obtained with `ALaDyn`. The parameters of the pulse are $\lambda_0 = 1\ \mu$m, $\Delta t_{\rm FWHM} = 15$ fs, $w_0 = 2\ \mu$m, and $Z_{\rm Rayleigh} = 12.6\ \mu$m ($= 42$ fs.) In the PIC simulation, we have taken nine points per wavelength in the longitudinal direction and three points per wavelength in the transversal ones.

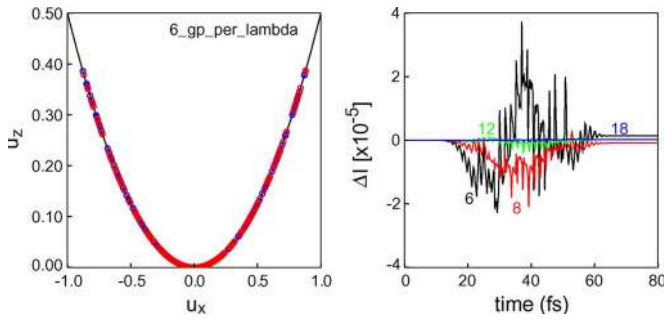

Fig. 5. (Left) Values of $u_x(t)$, $u_z(t)$ for two particles (red and blue circles) initially at rest (simulation with six grid points per wavelength). (Right) Plot of $\Delta I(t) \equiv I(t) - I(0)$ changing the number of grid points/wavelength from 6 to 18.

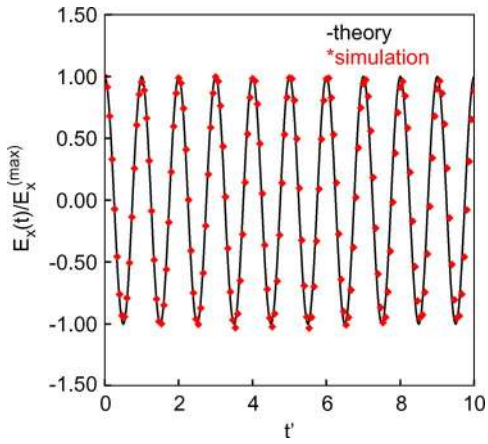

Fig. 6. Plasma oscillations. The black plot is the theoretical prediction, the red diamonds are the result obtained with `ALaDyn`. The simulation was performed with 200 particles/cell and 25 points per plasma wavelength.

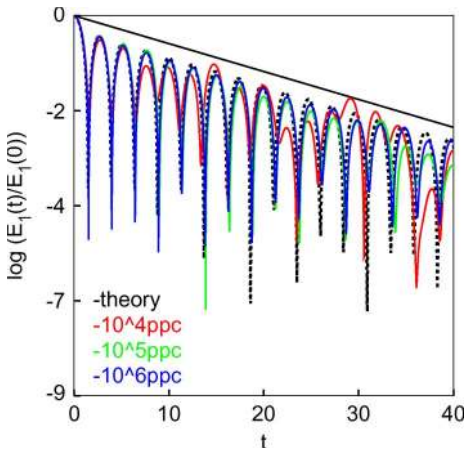

Fig. 7. Linear Landau damping. The solid black line is the theoretical damping rate; the dashed black plot is the behavior of $\log(E_1(t)/E_1(0))$ obtained with a Vlasov-fluid code with a grid of (512×1024) points. The remaining curves are the results obtained with `ALaDyn`, respectively, with (red) 10^4, (green) 10^5, and (blue) 10^6 particles/cell and a grid of 16 points.

of $u_x(t)$, $u_z(t)$ for two particles initially at rest. In the right panel, we plot the variation of the first integral, defined by $\Delta I(t) = I(t) - I(0)$, changing the number of grid points per wavelength. Again, with a coarse grid (eight to ten points/λ_0) the results are quite good.

C. Plasma Oscillations

Let us consider a uniform plasma ($n_0 = 2 \cdot 10^{19}$ electrons/cm^3) with a small perturbation in the density of $\sim$3%. The longitudinal electric field undergoes periodic oscillations at the plasma frequency $\omega_p^{(\rm th)} = 2.5229 \cdot 10^{14}$ rad/s. In Fig. 6, we show the normalized electric field $E/E_{\rm max}^{(\rm th)}$ as a function of the normalized time $t' = t\omega_p^{(\rm th)}/2\pi$. The simulation was performed with 200 particles/cell and 25 points per plasma wavelength, the time step was $dt = T_{\rm plasma}/15$. The value of the plasma frequency and the oscillation amplitude obtained from the simulation are both in good agreement with the theoretical ones. The numerical plasma frequency is found to be $\omega_p^{(\rm ALaDyn)} = 2.51 \cdot 10^{14}$ rad/s (relative error $< 0.4\%$).

D. Linear Landau Damping

This test deals with the linear Landau damping of a Langmuir wave in an electron/ion plasma. In the simulation, we consider a periodic domain in x; L is the periodicity. The ions are stationary, and the initial phase-space distribution for the electrons is

$$f_e(x, v, t=0) = (1 + \alpha \sin(kx)) \exp(-v^2/2)/\sqrt{2\pi}, \quad (10)$$

where $k \equiv 2\pi/L = 0.4$ and $\alpha = 0.02$. Here, and in the subsequent sections, time is normalized to the inverse of the electron plasma frequency ($\omega_{p,e}^{-1}$); space is normalized to the Debye length (λ_D) and velocity to the electron thermal speed ($\lambda_D \omega_{p,e}$). In Fig. 7, we show the behavior of $\log(E_1(t)/E_1(0))$, where E_1 is the amplitude of the fundamental harmonic of the electric field, obtained in different

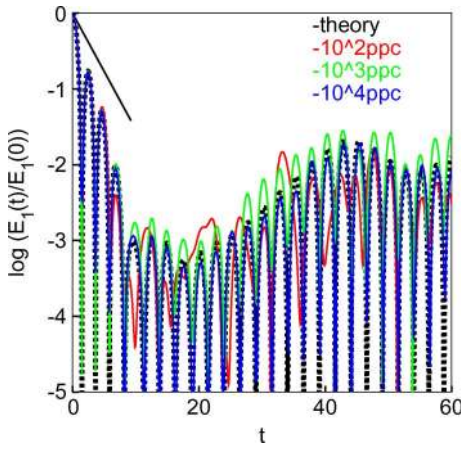

Fig. 8. Nonlinear Landau damping. The solid black line is the theoretical damping rate in the linear phase; the dashed black plot is the behavior of $\log(E_1(t)/E_1(0))$ obtained with a Vlasov-fluid code with a grid of (512 × 1024) points. The remaining curves are the results obtained with ALaDyn, respectively, with (red) 10^2, (green) 10^3, and (blue) 10^4 particles/cell and a grid of 32 points.

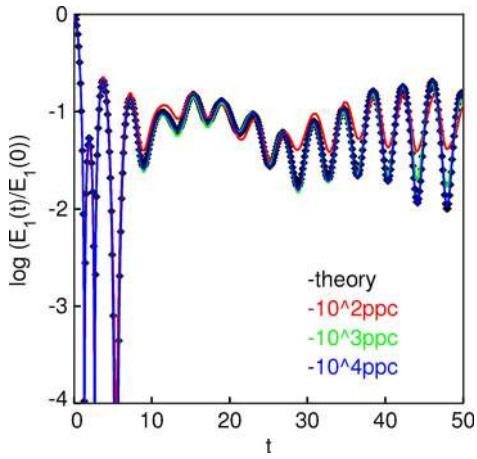

Fig. 9. Two-stream instability. The black plot is the behavior of $\log(E_1(t)/E_1(0))$ obtained with a Vlasov-fluid code with a grid of (512 × 1024) points. The remaining curves are the results obtained with ALaDyn, respectively, with (red) 10^2, (green) 10^3, and (blue) 10^4 particles/cell and a grid of 128 points.

simulations changing the number of particles per cell from 10^4 to 10^6 (see figure caption for details); the number of grid points is fixed to 16. The solid black line is the theoretical damping rate obtained from the linear-dispersion relation ($\gamma = 0.0661$), the dashed black plot is the result obtained with a Vlasov-fluid code with a grid of (512 × 1024) points. The linear-damping regime is valid as long as $0 \le t < t_{\text{bounce}} \equiv 2\pi\alpha^{-1/2} \simeq 40$. The linear Landau damping is a very "delicate" phenomenon from the numerical point of view. The agreement with theoretical results is quantitatively good only if the number of particles per cell is sufficiently large ($> 10^3$) to suppress the statistical noise.

E. Nonlinear Landau Damping

This test is similar to the previous one. The parameters are $k \equiv 2\pi/L = 0.5$ and $\alpha = 0.4$. In Fig. 8, we show the behavior of $\log(E_1(t)/E_1(0))$ obtained in different simulations, changing the number of particles per cell from 10^2 to 10^4 (see figure caption for details); the number of grid points is fixed to 32. The solid black line is the theoretical damping rate in the linear phase which ends at $t_{\text{bounce}} \equiv 2\pi\alpha^{-1/2} \simeq 10$. For $t > t_{\text{bounce}} \simeq 10$, we are well within the nonlinear phase [18]–[20]. The dashed black plot is the result obtained with a Vlasov-fluid code with a grid of (512 × 1024) points. We have a quantitative agreement with the Vlasov fluid using less particles per cell as compared to the previous case. Dealing, in this case, with large density perturbations, the statistical noise is not an issue.

F. Two-Stream Instability

We consider now the symmetric two-stream instability. In the simulation, we take a periodic domain in x (L is the periodicity). The ions are stationary, and the initial phase-space distribution for the electrons is

$$f_e(x,v,t=0) = \frac{e^{-\frac{(v-v_0)^2}{2\sigma^2}} + e^{-\frac{(v+v_0)^2}{2\sigma^2}}}{2\sqrt{2\pi\sigma^2}} (1 + \alpha \sin(kx)) \quad (11)$$

where $v_0 = 1.5$, $\sigma = 0.7$, $k \equiv 2\pi/L = 0.5$, and $\alpha = 0.4$. In Fig. 9, we show the behavior of $\log(E_1(t)/E_1(0))$ obtained in different simulations, changing the number of particles per cell from 10^2 to 10^4 (see figure caption for details); the number of grid points is fixed to 128. The black plot is the result obtained with a Vlasov-fluid code with a grid of (512 × 1024) points. As in the previous case, we have a quantitative agreement with the fluid solution with few particles per cell.

G. Electromagnetic Solitons in 1-D

We consider the behavior of an electromagnetic soliton in an electron–positron plasma [21]. The initial phase-space distributions compatible with a steady soliton are given by

$$f_e + (z,u_z) = f_e - (z,u_z) = \frac{\exp\left(-\beta\gamma(z,u_z)\right)}{2K_1(\beta)} \quad (12)$$

where $\gamma(z,u_z) = \sqrt{1+|a|^2+u_z^2}$, $a(z,t) = a_x(z,t) + ia_y(z,t) = a_0(z)\exp(i\omega t)$ is the (normalized) vector potential of the circularly polarized electromagnetic pulse, β is a free parameter, and $K_j(\cdot)$ is the modified Bessel function of the second kind of order j. The amplitude of the vector potential satisfies the following differential equation:

$$\frac{d^2a_0}{dz^2} + \omega^2 a_0 = 2a_0 \frac{K_0(\beta\sqrt{1+a_0^2})}{K_1(\beta)} \quad (13)$$

where ω is the laser frequency. The initial condition for a localized soliton is $a_0(0) = A_0$, $(da_0/dz)(0) = 0$, where A_0 is the solution of

$$\frac{1}{2}\omega^2 A_0^2 + \frac{2}{\beta}\left(\sqrt{1+A_0^2}\frac{K_1(\beta\sqrt{1}+A_0^2)}{K_1(\beta)} - 1\right) = 0. \quad (14)$$

We have considered the case with $\omega = 0.1$, $\beta = 100$, and $A_0 = 2$. In Fig. 10, we show the electron density when $t = 0$ (red) and when $t = 1000$ ($\simeq$ 159 plasma periods) (blue); the black line is the theoretical profile. We have considered two simulations; the number of particles per cell was, respectively,

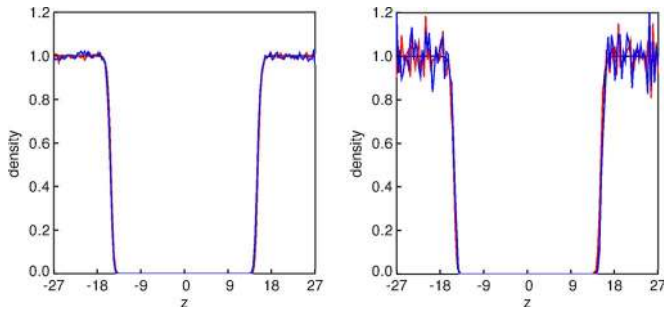

Fig. 10. Electromagnetic soliton with $\omega = 0.1$, $\beta = 100$, and $A_0 = 2$. Electron density profile (red) when $t = 0$ and (blue) when $t = 1000$ ($\simeq 159$ plasma periods). The black line is the theoretical value. The left panel refers to a simulation with 5000 particles/cell. The right panel to a simulation with 50 particles/cell. The number of grid points is fixed to 128.

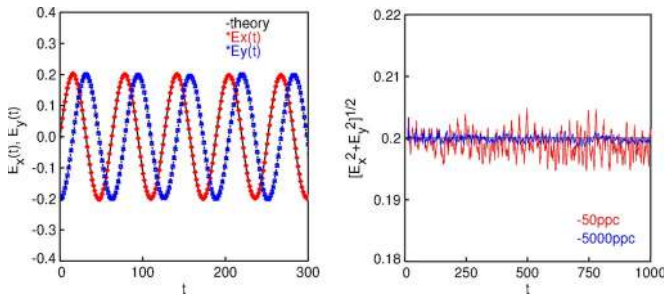

Fig. 11. Electromagnetic soliton with $\omega = 0.1$, $\beta = 100$, and $A_0 = 2$. (Left) Behavior of (red) $E_x(t)$ and (blue) $E_y(t)$ in the center of the soliton; the black line is the theoretical value. The number of particles per cell was 50 particles/cell. The number of grid points in the spatial grid is 128. (Right) Plot of the invariant $E = (E_x^2 + E_y^2)^{1/2}$ for the two simulations with, respectively, (red) 50 and (blue) 5000 particles/cell.

5000 (left plot) and 50 (right plot). The number of grid points is fixed to 128. The density profile remains stationary even with few particles per cell a part for the statistical fluctuations ($\sim 15\%$ in the right plot). In Fig. 11 (left panel), we plot the behavior of $E_x(t)$ (red) and $E_y(t)$ (blue) in the center of the soliton, for the simulation with 50 particles/cell. The black line is the theoretical prediction. The parameters are the same as in Fig. 10. In Fig. 11 (right panel), it is also shown that the behavior of the invariant $E = (E_x^2 + E_y^2)^{1/2}$ for the two simulations with 50 (red) and 5000 (blue) particles/cell. The invariant is well conserved in both cases a part for the intrinsic statistical noise. The maximum dissipation rate, due to the overall numerical collisionality, was registered in the second simulation (50 particles/cell) and is equal to $-1.35 \cdot 10^{-6}$.

H. Charge Conservation

In ALaDyn, electromagnetic fields are evolved using only Faraday and Ampère–Maxwell laws [(2)]. We recall that the remaining Maxwell equations [(4)] are automatically satisfied (and can be neglected) if, and only if, the continuity equation holds. In a PIC code, the introduction of the computational grid, the discretized representation of the operators $\nabla\cdot$, $\nabla\times$, $\partial/\partial t$, and the use of the shape function $S(\cdot)$ for the particles can lead to microscopic inconsistencies, violating the local charge conservation [12], [25]. To remove these inconsistencies, standard PIC codes [9]–[11] implement the charge-conserving current deposition scheme proposed in [25] and developed for a standard Yee lattice. Up to now, ALaDyn is not enforcing charge conservation, so *a priori*, there is no guarantee that Gauss' law is satisfied. We notice however that, in some of the previous benchmarks (e.g., linear/nonlinear Landau damping, two-stream instability), we tested basically the electrostatic aspects of our code, and the good agreement between PIC and Vlasov-fluid[2] results suggests that the code is correctly working. To investigate more in detail the reliability of the code from the point of view of the charge conservation, we have performed a 2-D simulation of the interaction of a laser pulse with a plasma (see Section V for details). During the simulation, we have compared the density distribution obtained weighting the particles on the computational grid and the one obtained by direct integration of the continuity equation ($\partial\rho/\partial t = -\nabla \cdot \mathbf{J}$). In Fig. 12, we show the particle (electron) density along the longitudinal (z) axis obtained with the particles weighting (black plot) and by direct integration of the continuity equation (red plot). The figures refer to two different times in the same simulation. No significant differences appear between the black and red plots in both figures. The main discrepancies are due to the statistical noise.

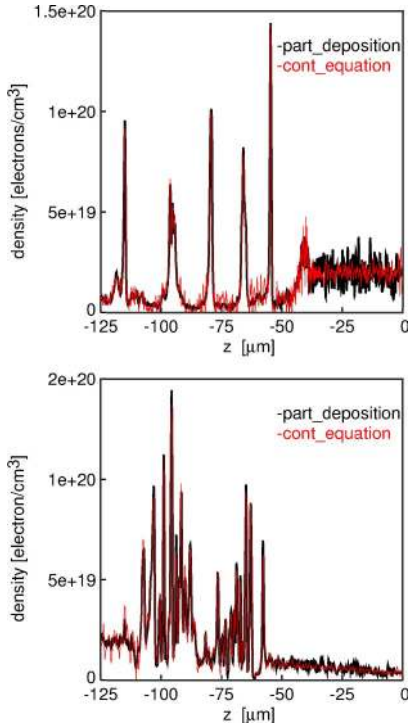

Fig. 12. Density distribution along z-axis obtained (black) weighting the particles and (red) by direct integration of the continuity equation. The two plots refer to two different times in the same simulation (see Section V for details).

V. Case Study

As a first application of ALaDyn, we consider an LWFA experiment. For the laser, we choose the parameters of the laser FLAME of the PLASMON-X experiment [7] (see Table I).

[2]In the Vlasov-fluid solver, we adopted for the benchmarks; the charge conservation is correctly enforced, since the electrostatic field is obtained directly from a spectral Poisson solver.

TABLE I
PARAMETERS OF THE LASER

Power (TW)	λ_0 (μm)	w_0 (μm)	Δt_{FWHM} (fs)
100	0.8	8	30

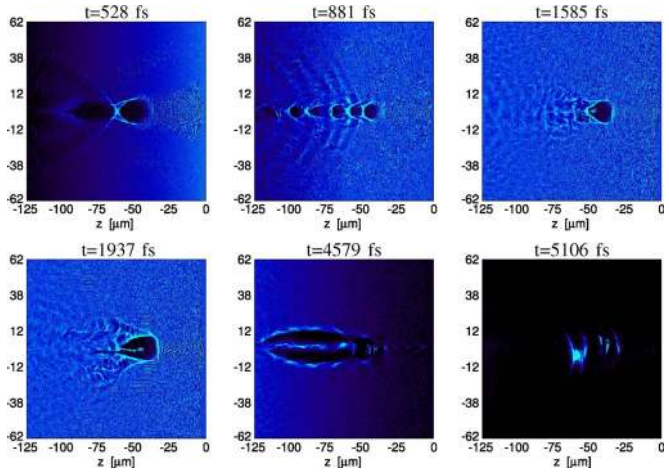

Fig. 13. Electron density during the simulation (see the text for details).

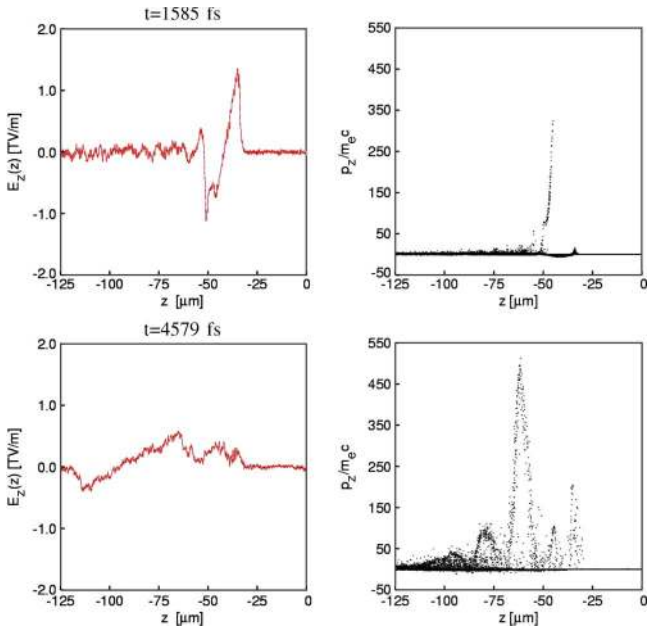

Fig. 14. (Left) Longitudinal electric field and (right) longitudinal phase space (z, p_z) for the electrons at two different times (see the text for details).

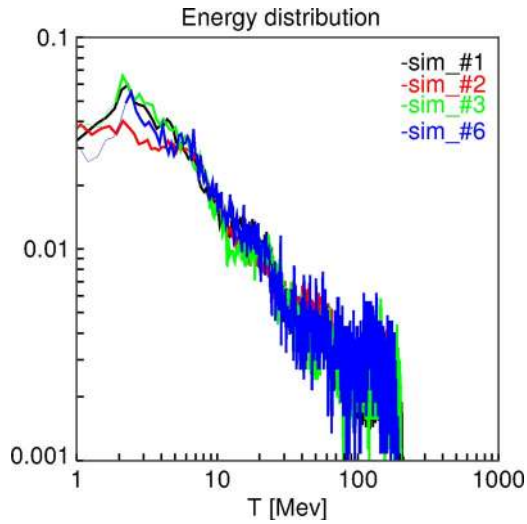

Fig. 15. Kinetic energy of the ejected electrons in different simulations changing the numerical parameters (mesh dimension, numerical particles) and fixing the physical ones.

The plasma has a flat-top profile with a length of 1.5 mm; the density in the plateau is $n_e = 2 \cdot 10^{19}$ electrons/cm^3. We have performed a 2-D simulation. The computational window was a square of (125 $\times$ 125) μm, and the mesh consisted of 1350 $\times$ 400 points, corresponding to approximately 9 $\times$ 3 grid points/wavelength. The velocity of the moving window was fixed to $0.98c$. The simulation used about $20 \cdot 10^6$ numerical-particles (electrons) corresponding to $\sim$40 particles/cell; we assumed that the ions are at rest. The spatial derivatives have been computed with an eighth-order compact scheme and the time integration with a Runge–Kutta scheme of the fourth order. The time step was chosen such that $c\Delta t = 0.67\Delta z$ in order to comply with the Courant condition. In Fig. 13, we show the evolution of the electron density with the formation of the bubble, the autoinjected electrons, and the accelerated bunch leaving the plasma. In Fig. 14 (left panel), we plot the electric fields and the longitudinal phase space (right panel) for the electrons at two different times. The maximum value of the longitudinal accelerating field is found to be $E_z \sim 1.0-1.3$ TV/m. From the linear theory, we obtain $E_z^{\max} \sim (\sqrt{n_e}/2)(a_0^2/2/\sqrt{a_0^2/2+1})$ (in volts per centimeter), and since for our laser-pulse $a_0 = 4.8$, we have $E_z^{\max} \sim 0.7$ TV/m, which is in agreement with the simulation. The electrons in phase with the accelerating field reach a peak energy of approximately 200–250 MeV. Finally, in Fig. 15, we show the energy spectrum of the ejected electrons obtained in four simulations, changing the numerical parameters (mesh dimension, numerical particles) and fixing the physical ones. No significant differences arise between the different simulations, ensuring the robustness of the numerical results.

VI. CONCLUSION

In this paper, we have presented ALaDyn, a relativistic fully self-consistent electromagnetic PIC code designed to study the laser–plasma interaction in 1-D, 2-D, and 3-D. The code, organized into a library of functions, is written in C and parallelized with MPI. It is based on high-order discretization methods (compact finite-differences schemes) for the differential operators in configuration space and on accurate time-integration schemes (high-order Runge–Kutta) ensuring high spectral accuracy. The goal is to use a coarser computational grid (allowing the use of a higher particles-per-cell number) and a larger time step as compared to standard PIC codes. The principal features of the code are as follows: flexibility in the definition of the plasma and of the laser pulse, implementation of the moving window, and implementation of the Lorentz boost technique. Several validation tests have already been made, and the benchmark with the PIC code VORPAL [9] is planned. ALaDyn was developed in the framework of the PLASMON-X collaboration and, during the period 2008–2010, will provide the simulation platform for the experiment.

ACKNOWLEDGMENT

The authors would like to thank Dr. P. Tomassini for useful discussions and suggestions.

REFERENCES

[1] T. Tajima and J. M. Dawson, "Laser electron accelerator," *Phys. Rev. Lett.*, vol. 43, no. 4, p. 267, Jul. 1979.
[2] W. P. Leemans *et al.*, "GeV electron beams from a centimetre-scale accelerator," *Nat. Phys.*, vol. 2, p. 696, 2006.
[3] I. Blumenfeld *et al.*, "Energy doubling of 42 GeV electrons in a metre-scale plasma wakefield accelerator," *Nature*, vol. 445, no. 7129, pp. 741–744, Feb. 2007.
[4] S. P. D. Mangle *et al.*, "Monoenergetic beams of relativistic electrons from intense laser plasma interactions," *Nature (London)*, vol. 431, no. 7008, p. 535, Sep. 2004.
[5] C. G. R. Geddes *et al.*, "High-quality electron beams from a laser wakefield accelerator using plasma-channel guiding," *Nature (London)*, vol. 431, no. 7008, p. 538, Sep. 2004.
[6] J. Faure *et al.*, "A laser–plasma accelerator producing monoenergetic electron beams," *Nature (London)*, vol. 431, no. 7008, p. 541, Sep. 2004.
[7] "CDR," *Plasma Acceleration and Monochromatic X-Ray Production.* [Online]. Available: http://ilil.ipcg.cnr.it/plasmoxn
[8] A. Pukhov, "Strong field interaction of laser radiation," *Rep. Prog. Phys.*, vol. 66, no. 1, pp. R47–R101, 2003.
[9] C. Nieter and J. R. Cary, "VORPAL: A versatile plasma simulation code," *J. Comput. Phys.*, vol. 196, no. 2, pp. 448–473, May 2004.
[10] R. A. Fonseca *et al.*, *OSIRIS: A Three-Dimensional, Fully Relativistic Particle in Cell Code for Modelling Plasma Based Accelerators*, vol. 2331. Berlin, Germany: Springer-Verlag, 2002, p. 342.
[11] A. Pukhov, "A laser Plasma accelerator producing monoenergetic electron beams," *J. Plasma Phys.*, vol. 61, p. 425, 1999.
[12] C. K. Birdsall and A. B. Langdon, *Plasma Physics via Computer Simulation*. Bristol, U.K.: A. Hilger.
[13] C. Benedetti *et al.*, "Numerical investigation of Maxwell–Vlasov equations part I: Basic physics and algorithms," *Commun. Nonlinear. Sci. Numer. Simul.*, vol. 13, no. 1, p. 204, Feb. 2008.
[14] S. K. Lele, "Compact finite difference schemes with spectral-like resolution," *J. Comput. Phys.*, vol. 103, p. 16, Nov. 1992.
[15] R. d'Inverno, *Introducing Einstein's Relativity*. London, U.K.: Oxford Univ. Press, 1992.
[16] J. L. Vay, "Noninvariance of space- and time-scale ranges under a Lorentz transformation and the implications for the study of relativistic interactions," *Phys. Rev. Lett.*, vol. 98, p. 130 405, Mar. 2007.
[17] L. D. Landau, "On the vibrations of the electronic plasma," *J. Phys. (Moscow)*, vol. 10, p. 25, 1946.
[18] F. Filbert and E. Sonnendrücker, "Comparison of Eulerian Vlasov solvers," *Comput. Phys. Commun.*, vol. 150, no. 3, pp. 247–266, Feb. 2003.
[19] G. Manfredi, "Long-time behavior of nonlinear landau damping," *Phys. Rev. Lett.*, vol. 79, no. 15, p. 2815, Oct. 1997.
[20] D. A. Gurnett and A. Bhattacharjee, *Introduction to Plasma Physics*. Cambridge, U.K.: Cambridge Univ. Press, 2005.
[21] M. Lontano *et al.*, "A kinetic model for the one-dimensional electromagnetic solitons in an isothermal plasma," *Phys. Plasma*, vol. 9, no. 6, p. 2562, Jun. 2002.
[22] Y. Elskens, "From long-range interaction to collective behaviour and from Hamiltonian chaos to stochastic models," *Nucl. Instrum. Methods Phys. Res., Sect. A, Accel. Spectrom. Detect. Assoc. Equip.*, vol. 561, no. 2, pp. 129–136, Jun. 2006.
[23] M. Calvo, J. M. Franco, and L. Randez, "A new minimum storage Runge–Kutta scheme for computational acoustics," *J. Comput. Phys.*, vol. 201, no. 1, pp. 1–12, Nov. 2004.
[24] D. L. Bruhwiler *et al.*, *Toward Quieter PIC Simulations of LWFA Experiments with the VORPAL Code*. these Proceedings.
[25] J. Villasenor and O. Buneman, "Rigorous charge conservation for local electromagnetic field solvers," *Comput. Phys. Commun.*, vol. 69, no. 2/3, pp. 306–316, Mar. 1992.

Carlo Benedetti was born in 1978. He received the B.S. and Ph.D. degrees in physics from the University of Bologna, Bologna, Italy, in 2002 and 2006, respectively.

He is currently a Research Fellow with the Department of Physics, University of Bologna, associated with the INFN (Bologna Section). His current main interests include the theory and simulation of laser–plasma interaction, as well as the development of algorithms and numerical codes for the simulation of many-particle systems.

Andrea Sgattoni was born in 1982. He received the B.S. and M.S. degrees in physics from the University of Bologna, Bologna, Italy, in 2004 and 2007, respectively, where he defended a thesis on the ponderomotive acceleration of electrons via laser–plasma interaction.

He is currently with the Department of Physics, University of Bologna, associated with the INFN (Bologna Section). His current main interests include the theory and simulation of laser–plasma interaction.

Giorgio Turchetti was born in 1942. He received the degree in physics from the University of Bologna, Bologna, Italy in 1965.

He is currently a Professor of mathematical physics with the Department of Physics, University of Bologna, and the Coordinator of research activities on the physics of complex systems. He is also the Director of the Center for Biophysics and Biocomplexity "L. Galvani." He is the author of about 200 papers published in refereed journals. His recent research activity is devoted to beam dynamics via laser–plasma acceleration and modeling of complex systems.

Pasquale Londrillo was born in 1942. He received the degree in physics from the University of Bologna, Bologna, Italy, in 1965.

From 1969 to 1982, he was a secondary school teacher. He is currently a Researcher in astronomy with the L'Istituto Nazionale di Astrofisica (INAF), Osservatorio Astronomico di Bologna, Bologna. He is the author of nearly 40 referenced published papers. His main interest includes computational magnetohydrodynamics, plasma physics, and gravitational N-body systems.